Synthesis Imaging in Radio Astronomy II
ASP Conference Series, Vol. XXX, 1998
G.B. Taylor, C.L. Carilli, and R. A. Perley (eds.)

3. The Primary Antenna Elements

P.J. Napier
National Radio Astronomy Observatory, Socorro, NM, USA, 87801

Abstract. The primary antenna elements are one of the most important pieces of equipment in a synthesis telescope. Because the performance properties of the antennas can affect the quality of the synthesized images in a number of fundamental ways, the relevant antenna design and performance parameters are reviewed in this chapter.

1. Introduction

In this chapter I describe the design and performance of the primary antenna elements which are used to sample the electromagnetic field radiated by the observed radio source. In general, throughout these chapters, few details are given of the equipment that is used in synthesis arrays. It is appropriate, however, to treat the antenna elements more completely because of the many ways in which they can directly affect the quality of the images produced by the array. The important properties of the primary antenna that can affect the image include aperture efficiency, pointing accuracy, beam circularity, sidelobe level, polarization purity and noise temperature. The techniques needed to achieve good antenna performance with respect to these parameters can be found in the modern antenna engineering literature (see, for example, Rudge et al., 1982; Kraus, 1988; Olver et al., 1994; Balanis, 1997) so I will not give details in this chapter. Instead, I shall emphasize why these parameters are important.

Figure 3-1 shows a simple block diagram of the major pieces of equipment required in a synthesis telescope. For the purposes of this chapter I will define the primary antenna element to be the piece of equipment that intercepts the propagating electromagnetic wave from the observed source and makes a sample of it available at the input to the first low-noise amplifier, either as an electric current on a cable or as a field in a single-mode waveguide. Thus, for reflector antennas, I include the feed and its polarization splitter as part of the antenna. At the output of the antenna the signal is at the radio, or sky, frequency ν_{RF}. As shown in Figure 3-1, the signal undergoes various frequency translations as it propagates through the electronics system. In this chapter I will not be concerned with any of the equipment after the antenna. The correlator is treated in detail in Lecture 4, and a discussion of the importance of the noise temperature of the receiver is given in Lecture 4. In general the receiver, intermediate frequency, transmission line, local oscillator and baseband portions of the electronics system all have the requirement of good amplitude and phase stability. These requirements and others such as bandpass shape control, low spurious signal generation and good signal isolation are discussed in references such as Napier, Thompson and Ekers (1983) and Thompson, Moran and Swenson (1986).

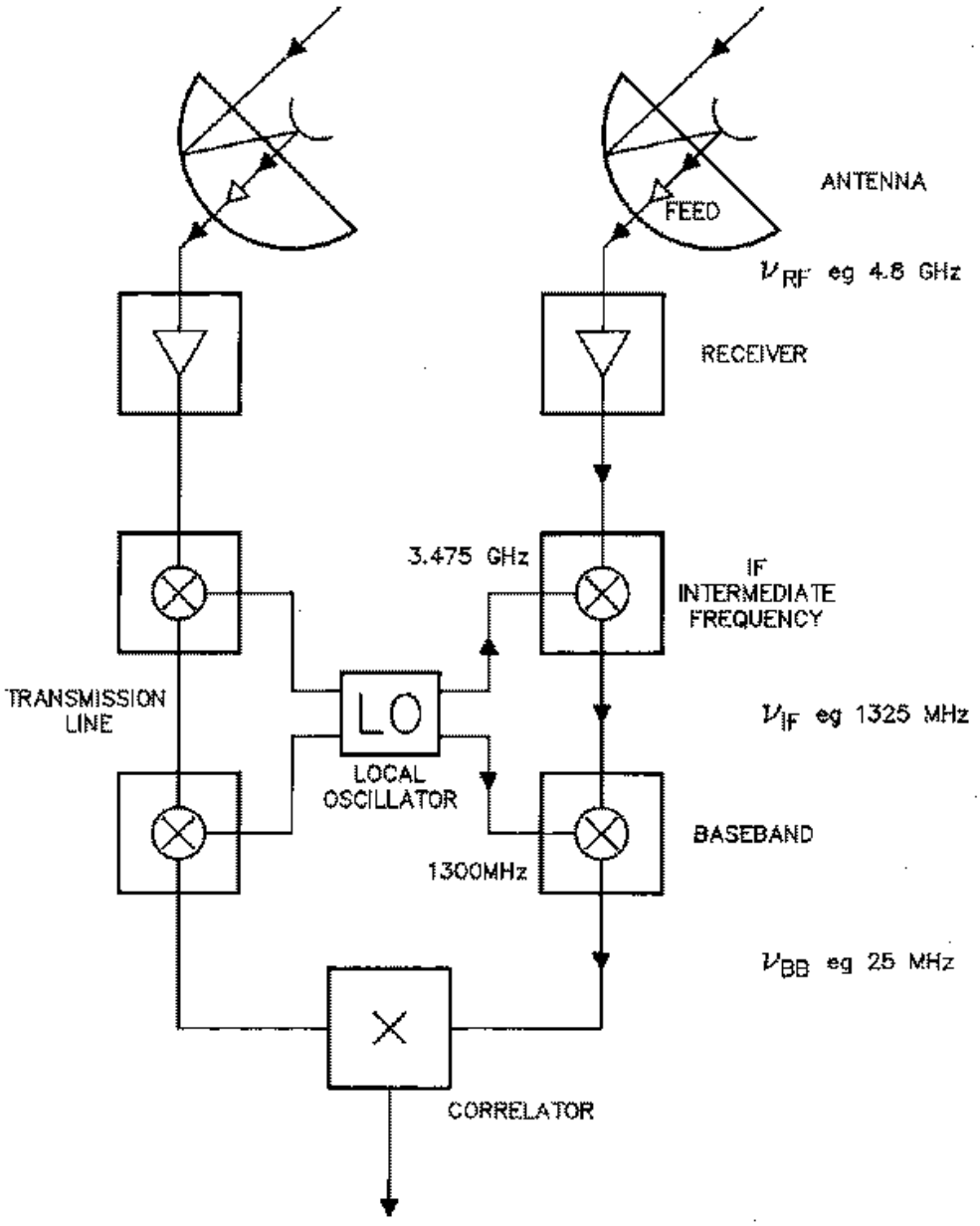

Figure 3-1. A simplified block diagram of the electronic equipment used to produce the correlation from one antenna pair in a synthesis telescope. The signal frequencies given as examples at various points through the electronics chain are typical of the VLA observing at 4.8 GHz.

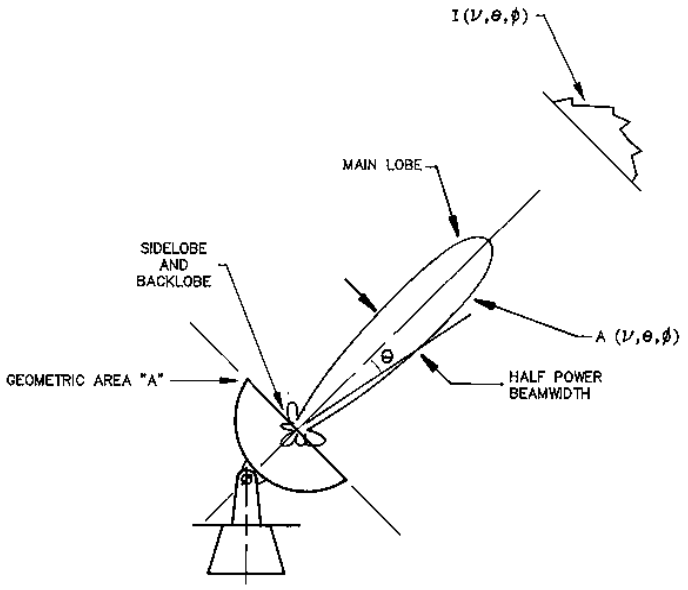

Figure 3-2. The reception pattern of an antenna.

2. Basic Antenna Formulas

In this section I introduce a few standard antenna formulas which will be useful in understanding how the properties of the primary antenna element affect a synthesized image. Derivation of these expressions can be found in standard textbooks (e.g., Kraus 1986, Chapter 3).

We require the concept of the effective collecting area of the primary antenna $A(\nu, \theta, \phi)$ (in units of m^2), where ν is frequency and θ and ϕ are direction coordinates. If the antenna is pointed at a source with brightness $I(\nu, \theta, \phi)$ $\mathrm{W\,m^{-2}\,Hz^{-1}\,sr^{-1}}$ (see Figure 3-2), then the power P (in watts) received by the antenna in bandwidth $\Delta\nu$ from element $\Delta\Omega$ of solid angle is given by

$$P = A(\nu, \theta, \phi) I(\nu, \theta, \phi) \Delta\nu \Delta\Omega \; . \tag{3-1}$$

The normalized antenna reception pattern $\mathcal{A}$, or power pattern as it is often called, is defined as

$$\mathcal{A}(\nu, \theta, \phi) = A(\nu, \theta, \phi)/A_0 \; , \tag{3-2}$$

where A_0 (m^2) is the response at the center of the main lobe of $A(\nu, \theta, \phi)$ and is called the effective area of the antenna. The beam solid angle, Ω_A, of the power pattern is defined as

$$\Omega_A = \int\int_{allsky} \mathcal{A}(\theta, \phi)\, d\Omega \, . \tag{3-3}$$

An important fundamental relationship in antenna theory states that the product of the effective area and the beam solid angle is equal to the square of the wavelength (Kraus 1986, page 6–5),

$$A_0 \Omega_A = \lambda^2 \, . \tag{3-4}$$

Ω_A is a measure of the field of view of the synthesis telescope. If $\mathcal{A}$ is everywhere equal to 1, then Ω_A has its maximum possible value of 4π and the primary antenna is isotropic and can see the whole sky with equal sensitivity. In this case the synthesis telescope could in principle make an image of the whole sky all at once. A large field of view is desirable, but Relationship 3-4 shows that, for any given frequency, when Ω_A is a maximum, A_0 is a minimum and so the power received is also a minimum. This means that the sensitivity is at a minimum. As the collecting area is increased to improve sensitivity, Relationship 3-4 dictates that the field of view necessarily decreases. This tradeoff between field of view and sensitivity has to be made when selecting the size of the primary antenna elements for any synthesis telescope. It requires consideration of the size/cost curve for the antennas and the expected size and spectral index properties of the radio sources to be observed.

For antennas that have a well defined physical collecting area, such as reflector, lens or horn antennas, the ratio of A_0 to the physical area A of the aperture is called the aperture efficiency η, a dimensionless quantity less than unity:

$$A_0 = \eta A\,. \tag{3-5}$$

The final antenna relationship that we will find useful is the Fourier transform relationship between the complex voltage distribution of the field, $f(x, y)$, in the aperture of an antenna and the complex far-field voltage radiation pattern, $F(u, v)$, of the antenna (Kraus 1986, Section 6–8):

$$F(u,v) = \int\int_{aperture} f(x,y) e^{2\pi i(ux+vy)}\, dx\, dy\,, \tag{3-6}$$

and

$$f(x,y) = \int_{-\infty}^{\infty}\int_{-\infty}^{\infty} F(u,v) e^{-2\pi i(ux+vy)}\, du\, dv\,. \tag{3-7}$$

Figure 3-3 shows the form of $f(x, y)$ and $F(u, v)$. The radiation pattern coordinates are given by

$$u = \frac{\sin\theta\cos\phi}{\lambda} \quad \text{and} \quad v = \frac{\sin\theta\sin\phi}{\lambda}\,. \tag{3-8}$$

The voltage and power patterns are related by $\mathcal{A} = |F|^2$. The Fourier transform relationship between an antenna aperture distribution and its radiation pattern is analogous to the one between the source brightness distribution and its visibility function. In the analogy, aperture distribution and brightness distribution are the analogous quantities because they both are of compact support,[1] although the analogy is not perfect because the aperture distribution is complex whilst brightness is real. Both antenna radiation pattern and source visibility function have the same general form of a main central lobe surrounded by lesser sidelobes, but the radiation pattern does not have to be Hermitian (i.e., need not be conjugate symmetric).

[1] This is not strictly so in the case of the brightness distribution, but it is essentially so.

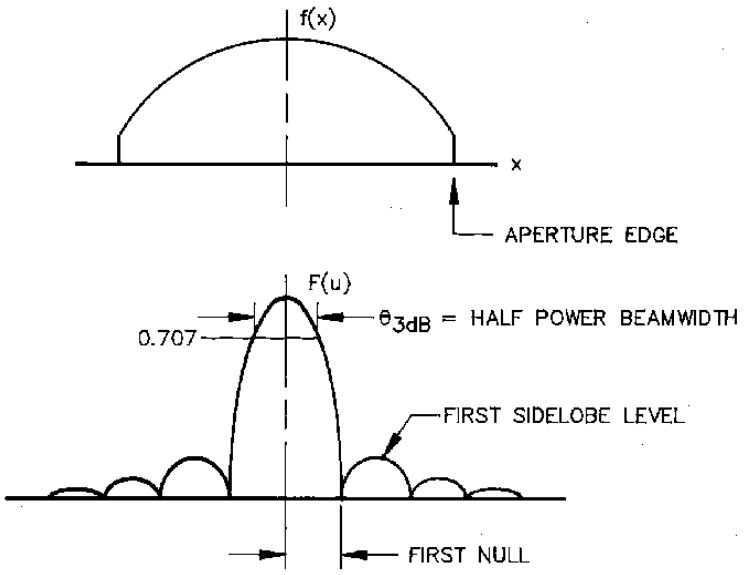

Figure 3-3. The Fourier transform relationship between an antenna aperture distribution and its far-field radiation pattern. The form of the aperture distribution, $f(x)$, and the radiation pattern, $F(u)$, are shown for a one-dimensional example. In general both quantities are complex. Only the amplitudes are shown here.

The form of $f(x, y)$ for an antenna is determined by the way in which the antenna feed illuminates the aperture. In general, the more that $f(x, y)$ is tapered at the edge of the aperture, the lower will be the aperture efficiency and the sidelobes and the broader the main beam. Tabulations of a wide variety of $f(x, y)$, and their $F(u, v)$, can be found in antenna textbooks (Hansen 1964, p. 66; Rudge *et al.* 1982, Table 1.2). For example, the VLA antennas are designed to have uniform illumination ($f(x, y) = constant$) over the whole aperture, except where the aperture is blocked by the subreflector and its support struts. In this case, for a circularly symmetric aperture of diameter D, $F(u) = J_1(\pi Du)/u$, which has the properties: first sidelobe level = -17.6 dB, half power beamwidth = $1.02\lambda/D$, and position of first null = $1.22\lambda/D$. These are in good agreement with measured beam parameters for the VLA 25-meter diameter reflector, except for the first sidelobe level, which is modified by aperture blockage as shown in Figure 3-8.

3. General Antenna Types

In this section I will discuss some of the general considerations that determine the selection of a primary antenna element for a synthesis array.

3.1. Wavelength range

The most important factor governing the selection of the primary antenna element is the frequency range to be observed by the synthesis telescope. Typically,

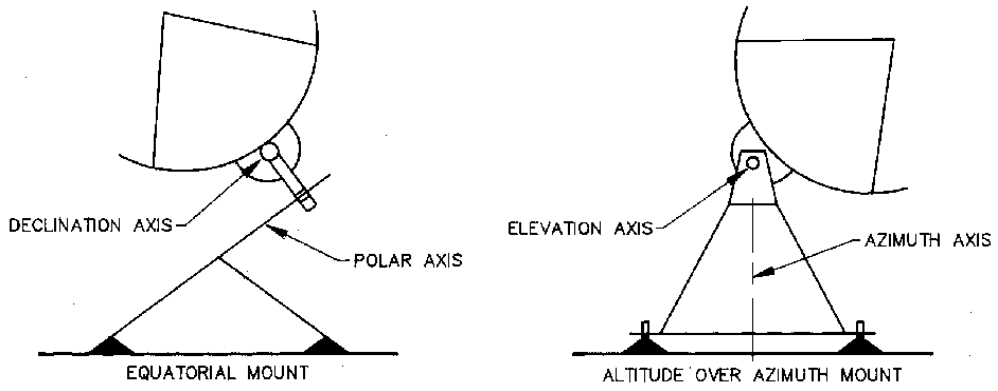

Figure 3-4. Equatorial and Altazimuth antenna mounts.

for wavelengths longer than about 1 m, wire antennas are used. These include dipoles, yagis, spirals and helices. Sometimes small arrays of these elements are used to increase collecting area. For wavelengths shorter than approximately 1 m, reflector antennas are common, and occasionally horn antennas are used for very wide field of view instruments. The changeover frequency from wire to reflector antennas is not sharply defined, and, around 1-m wavelength, combinations of the two types can be found. Thus the Molonglo Synthesis Telescope at 800 MHz uses a cylindrical paraboloidal reflector with a reflective surface formed with parallel wires, and the VLA at 75 MHz uses a solid 25-m diameter reflector fed by a simple wire crossed dipole. References for the different antenna elements that have found application in synthesis telescopes can be found in the comprehensive listing of synthesis arrays given in Napier, Thompson and Ekers (1983).

Since wire antennas are simpler and less expensive to build than reflector antennas one might ask why they are not used at all wavelengths. The answer is contained in Equation 3-4. As an antenna design is scaled from one wavelength to another, so that its pattern $\mathcal{A}$ is the same, its collecting area increases as λ^2. Thus, whilst wire antennas have sufficient collecting area to be useful at long wavelengths, they are too small to be primary elements at short wavelengths. Since most of the currently active synthesis telescopes use reflector antennas I will concentrate on them for the rest of this chapter.

3.2. Types of reflector antennas

The two major choices that have to be made when designing a reflector antenna for use in a synthesis array are the choice of mount and the choice of optics.

Choice of mount The choice of the mount is usually between an equatorial mount and an elevation-over-azimuth (altazimuth) mount, as shown in Figure 3-4. The elevation-over-azimuth mount has the advantage of simplicity and hence lower cost. Gravity always acts on the reflector in the same plane, and this eases the problem of designing to keep the reflector profile accurate as the antenna tracks an astronomical source. The major disadvantage of this mount is that, as

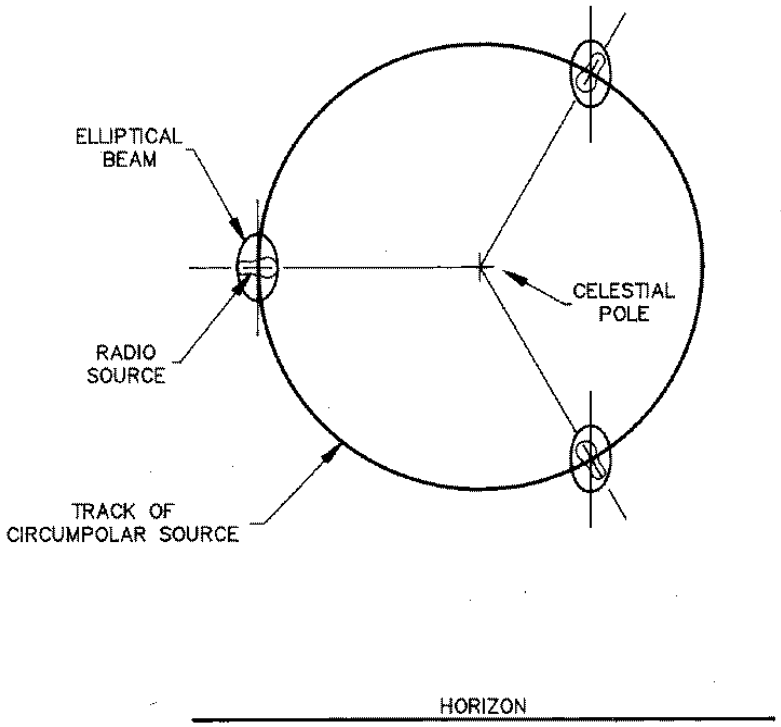

Figure 3-5. Demonstration of the rotation of the beam of an altazimuth antenna with respect to an astronomical source. A circumpolar double-lobed source, extended in the North–South direction, is shown at three different hour angles. The antenna beam is extended in the vertical direction.

the antenna tracks, the aperture rotates with respect to the source (Thompson, Moran and Swenson 1986, p. 97). This rotation is about the line from the center of the aperture to the source and means that the antenna beam rotates with respect to the source. If the source size is of the order of the beam size, and if the beam is not circularly symmetric, this rotation will cause the apparent brightness distribution to vary. Figure 3-5 gives a simple demonstration of this effect. Since aperture blockage usually makes the beam sidelobe pattern non-circularly symmetric, and the antenna instrumental polarization is not circularly symmetric, the dynamic range of total intensity images of very large sources and polarization images of extended sources will be limited by this effect. Observers of extended sources need to consider this effect when judging the fidelity of subtle features in the images of these sources. Another minor disadvantage of this mount is that a source passing close to the zenith of the antenna cannot be tracked near the zenith because of the high rates of azimuth rotation needed.

The equatorial mount has the advantage that, since the polar axis is aligned parallel to the axis of rotation of the Earth, rotation about this single axis is adequate to track an astronomical object moving at sidereal rate. Its principal advantage is that it does not suffer from the beam rotation problem discussed above for the alt–az mount. The principal disadvantage is that as the reflector tracks, gravity does not act always in the same plane. This, together with the

inclined polar axis, significantly increases the complexity of the design, with a resulting increased cost. A minor disadvantage of this mount is that it cannot observe sources close to the horizon in the direction away from the celestial pole.

A final important point is that, irrespective of what type of mount is chosen, it is important that antenna structures be made as identical as possible between different elements of the array. This will minimize the effect of many kinds of deformations and other errors, or at least make it easier to calibrate them.

Choice of optics There are a number of different optical systems that can be used to feed a large radio reflector (Rudge et al. 1982, Section 3.6). Figure 3-6 shows some of the feed systems that have been used for radio telescope reflectors. The *prime focus system* (as in the Westerbork Synthesis Telescope) has the advantage that it can be used over the full frequency range of the reflector, including the lowest frequencies where secondary focus feeds become impractically large. The disadvantages of the prime focus are that space for, and access to, the feed and receiver is restricted and spillover noise from the ground decreases sensitivity. All of the *multiple reflector systems* (Figure 3-6(b)–(f)) have the advantage of more space, easier access to the feed and receiver, and reduced noise pickup from the ground. In addition, the primary and secondary reflectors can be shaped to provide more uniform illumination in the main reflector aperture, as described in Section 4.1.

The *off-axis Cassegrain* (e.g., in the VLA and VLBA) is particularly suitable for synthesis telescopes needing frequency flexibility, because many feeds can be located in a circle around the main reflector axis so that changing frequency simply requires a rotation of the subreflector around this axis. The disadvantage of this geometry is that the asymmetry degrades polarization performance. The *Naysmith geometry* (e.g., the Owens Valley Millimeter Array) provides a receiver cabin external to the antenna structure, whilst the *beam waveguide feed* (e.g., the Nobeyama 45-m millimeter wavelength telescope) provides maximum convenience by locating the feeds and receivers at ground level. The *offset Cassegrain* (e.g., the Bell Labs millimeter telescope) has no blockage and so can have a circularly symmetric beam with low sidelobes. This makes it an attractive choice for wide field-of-view synthesis telescopes, but the increased complexity of reflector panel tooling and subreflector support structure leads to increased cost.

4. Antenna Performance Parameters

In this section I discuss some of the performance parameters of primary antenna elements that can directly affect the quality of images made with synthesis telescopes.

4.1. Aperture efficiency

The antenna aperture efficiency, defined in Equation 3-5, directly impacts the sensitivity of the synthesis telescope (Lecture 9). The aperture efficiency, η, is the product of a number of different loss factors,

$$\eta = \eta_{sf}\,\eta_{bl}\,\eta_s\,\eta_t\,\eta_{misc}\,, \tag{3-9}$$

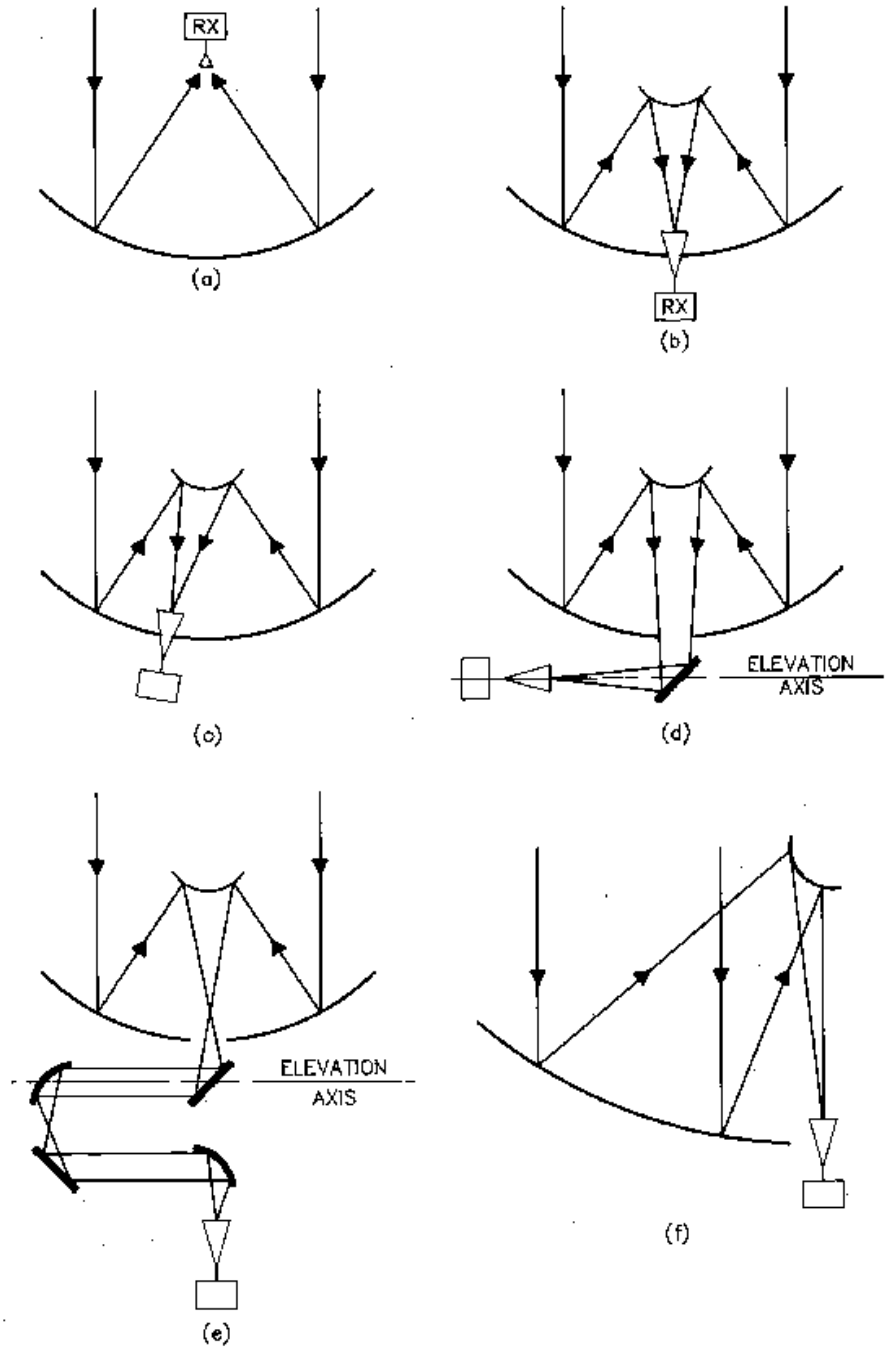

Figure 3-6. Optical systems for radio telescope reflectors. **(a)** Prime focus, **(b)** Cassegrain, **(c)** Off-axis Cassegrain, **(d)** Naysmith, **(e)** Beam waveguide, **(f)** Offset Cassegrain.

where η_{sf} = reflector surface efficiency, η_{bl} = reflector blockage efficiency, η_s = feed spillover efficiency, η_t = illumination taper efficiency, and η_{misc} = miscellaneous efficiency losses due to reflector diffraction, feed position phase errors, and feed match and loss.

Surface efficiency This factor accounts for aperture efficiency loss due to inaccuracies in the reflector profile. If the reflector has errors, then the electric field from different parts of the aperture will not add together perfectly in phase at the feed, leading to a decrease in received power. Ruze (1966) gives an expression for surface efficiency

$$\eta_{sf} = e^{-(4\pi\sigma/\lambda)^2}, \tag{3-10}$$

where σ is the r.m.s. surface error, with the errors assumed to be random from a Gaussian population and uncorrelated from one point to another in the aperture. In a Cassegrain system σ is an appropriately defined composite r.m.s. error of the primary and secondary reflector surfaces. If the errors are correlated over significant fractions of the aperture, then additional terms are required on the right hand side of Expression 3-10 (Ruze 1966). Expression 3-10 predicts that for an r.m.s. error of $\lambda/16$, $\eta_{sf} = 0.54$, which is often taken as the useful upper frequency limit for a reflector. As well as the loss of sensitivity resulting from a low value of η_{sf}, one has to be concerned with the quality of the primary beam. Ruze (1966) shows that the surface errors produce a broad scatter pattern that surrounds the main lobe of the beam and can be higher than the usual diffraction-limited sidelobes. This scatter pattern could enhance image artifacts caused by sources near the primary beam. For a reflector of diameter D, if the reflector errors are correlated over distances D/N then the scatter pattern will be N times broader than the diffraction-limited main lobe. Figure 3-7 shows the scatter pattern for surface errors of size $\lambda/16$ r.m.s. and $N = 10$, as might be the case, for example, if the errors are due to incorrect alignment of otherwise accurate reflector panels.

Good η_{sf} performance requires careful structural design for wind, thermal and gravitational loading, together with precise reflector panels and an accurate panel setting technique.

Aperture blockage The feed or subreflector and its multi-legged support structure block the aperture of a reflector antenna, as shown in Figure 3-8. This typically results in a blockage efficiency in the range $0.75 < \eta_{bl} < 0.95$. η_{bl} is given (Rudge et al. 1982, p. 179) by

$$\eta_{bl} = \left(1 - \frac{effective\ blocked\ area}{total\ area}\right)^2. \tag{3-11}$$

The effective blocked area is the blocked area weighted for the illumination taper in the aperture. Similarly, the total area is weighted for the illumination taper in the aperture. Equation 3-11 shows, for small blockage, that the loss in efficiency is twice the fractional blocked area. As well as the loss in aperture efficiency, the increase in antenna beam sidelobe level due to blockage is important for synthesis telescopes. Using the Fourier transform relationship of Equation 3-6, the form of the antenna voltage pattern with blockage can be calculated as the unblocked voltage pattern minus the voltage patterns of the

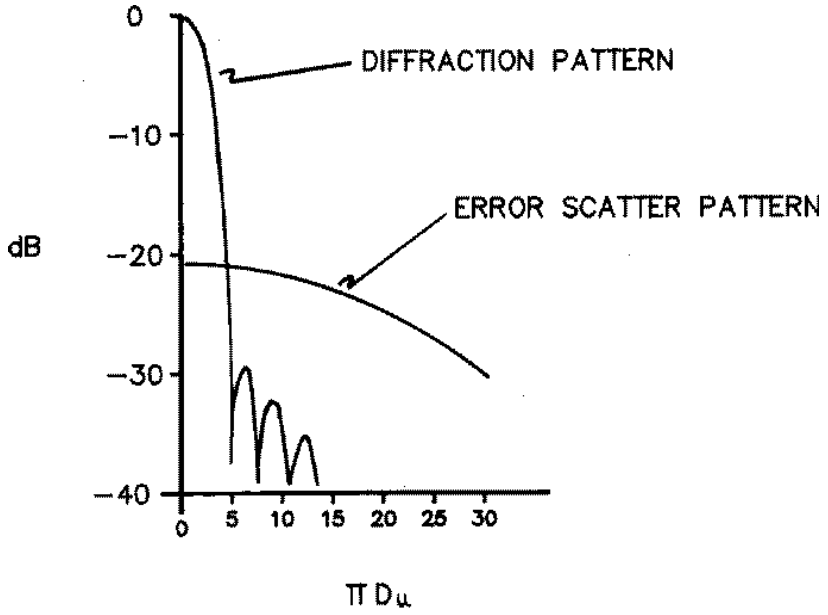

Figure 3-7. Diffraction pattern and surface error scatter pattern for r.m.s. surface errors $\lambda/16$ correlated over distances $D/10$. The aperture has a -12 dB edge taper. The total pattern is the power sum of the diffraction and error patterns. [From Ruze 1966.]

blocked areas. This is shown in Figure 3-8, where the typical pattern of enhanced sidelobes in planes orthogonal to the subreflector support legs can be seen.

Feed spillover efficiency This effect can most easily be understood by considering the antenna in transmission, rather than reception mode. The feed spillover efficiency is the fraction of the power radiated by the feed that is intercepted by the subreflector for a Cassegrain feed, or by the main reflector for a prime focus system. Clearly, power that does not intercept the reflector is lost, and we can be confident that a similar loss occurs in reception mode by invoking the Reciprocity Principle (Rudge et al. 1982, p. 11). η_s is given (Rudge et al. 1982, p. 170) by

$$\eta_s = \frac{\int_0^{2\pi}\int_0^{\theta_R} P_f(\theta,\phi)\sin\theta\, d\theta\, d\phi}{\int_0^{2\pi}\int_0^{\pi} P_f(\theta,\phi)\sin\theta\, d\theta\, d\phi}, \tag{3-12}$$

where $P_f(\theta,\phi)$ is the power pattern of the feed and θ_R is the angle subtended by the reflector (see Figure 3-9). η_s increases as $P_f(\theta_R)$ is reduced, but η_t decreases, so a tradeoff between spillover and illumination efficiency must be made. The shaped reflector systems discussed in the next section ease this problem. Typically, $0.70 < \eta_s < 0.97$, with the higher values requiring shaped reflectors. As well as the loss of sensitivity, the impact of spillover on the sidelobes of the antenna must be kept in mind. At θ_R, the gain of the feed may be well above the diffraction sidelobes of the primary aperture, causing higher than expected antenna sidelobes at distance θ_R away from the peak of the main beam. This

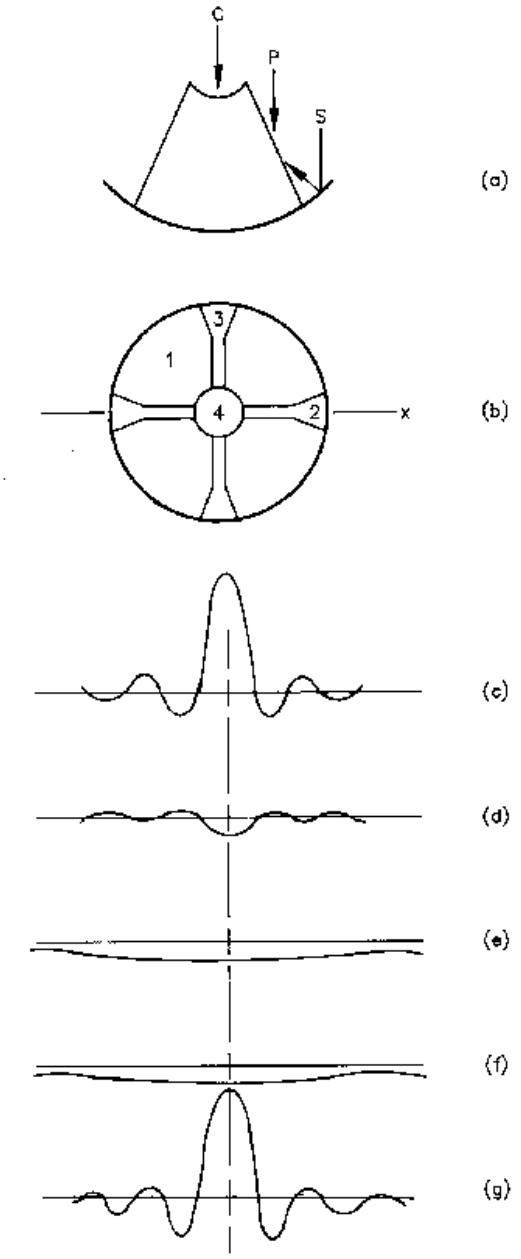

Figure 3-8. Effect of aperture blockage. **(a)** The three kinds of blockage in a reflector. c is central blockage, p is plane wave blockage on the struts, and s is spherical wave blockage on the struts. **(b)** The resulting aperture blockage for a quadrupod subreflector support. **(c)** Unblocked pattern in x-plane. **(d)** Blocked pattern for area 2. **(e)** Blocked pattern for area 3. **(f)** Blocked pattern for area 4. **(g)** Total pattern with blockage $= c + d + e + f$.

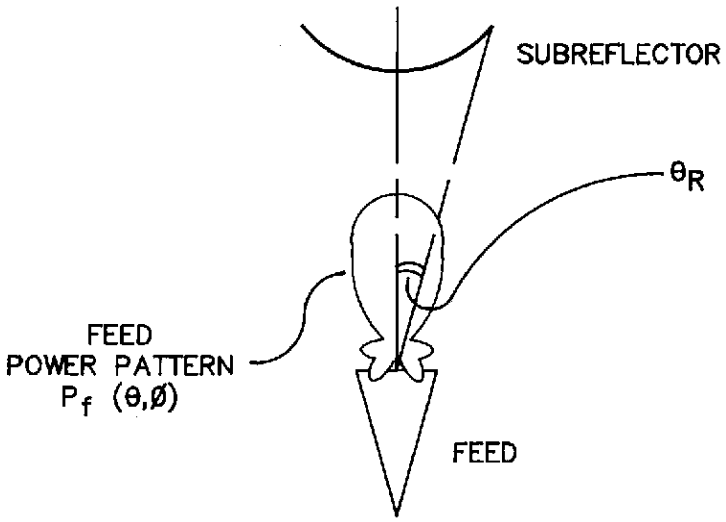

Figure 3-9. Feed spillover.

problem is worst at the lowest frequency, where the gain of the primary aperture is lowest. For example, for the VLA at $\lambda = 21$ cm, the feed spillover past the subreflector is about 20 dB higher than the diffraction-limited sidelobes at a distance $\theta_R = 9°$ off the peak of the beam. This effect can enhance the effect of confusing sources outside the expected field of view of the synthesis image.

Illumination taper efficiency Illumination taper efficiency accounts for the loss in collecting area due to the fact that the feed pattern usually illuminates the outer parts of the primary reflector at a lower level than the inner part. η_t is given (Rudge et al. 1982, p. 171) by

$$\eta_t = \frac{\left(\int\int_{aperture} |f(x,y)|\,dx\,dy\right)^2}{A\int\int_{aperture} |f(x,y)|^2\,dx\,dy}\,. \tag{3-13}$$

η_t equals 1 for uniform illumination ($f(x,y) \equiv 1$). Typically, to prevent η_s from being too low, an illumination taper of about 10 dB is used at the edge of the aperture, which results in a η_t in the range 0.7 to 0.8. This can be improved significantly if a shaped Cassegrain (Rudge et al. 1982, p. 247) reflector system is used. With this technique, the subreflector is deformed slightly from the usual hyperbolic shape in such a way that the feed pattern, after reflection from the subreflector, is significantly modified, with increased illumination at the edge of the aperture (see Figure 3-10). Since the shape of the subreflector is altered, the main reflector must also be modified slightly from a paraboloid to avoid aperture phase errors. Using this technique, values of η_t close to 1 can be achieved with reflector edge tapers in the range -15 dB to -20 dB. The resulting $\eta_t\eta_s$ product can be 20% to 30% better than with unshaped systems.

Some disadvantages of shaped Cassegrain geometries, which do not usually preclude their use for synthesis telescopes, include increased sidelobes due to the uniform illumination, no prime focus operation above a frequency of about

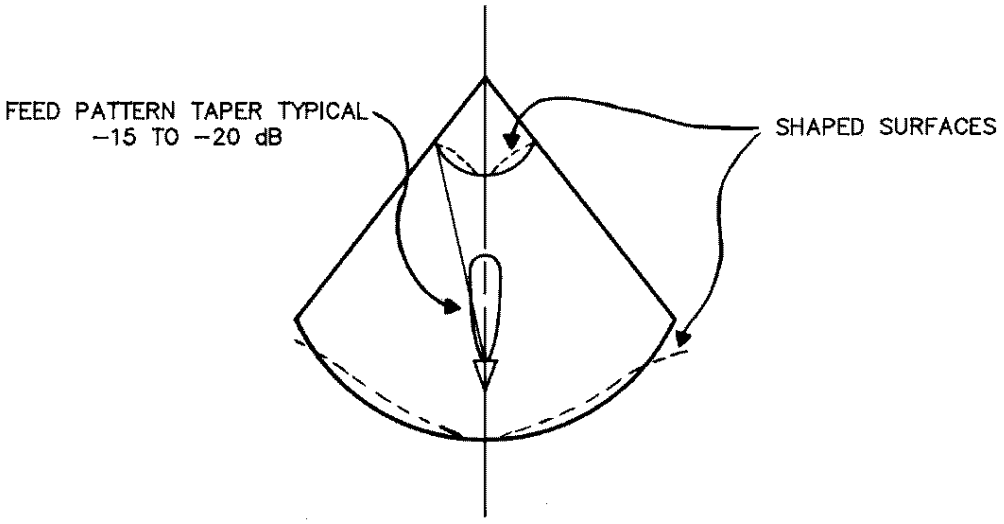

Figure 3-10. Shaped Cassegrain reflector system. The subreflector is deformed to increase illumination at the edge of the main reflector.

1 GHz because of the shaped main reflector, and very bad beam degradation if the feed is moved away from the secondary focal point. This latter problem may be a limitation for synthesis arrays intended to obtain very wide fields of view by using multiple feeds. An interesting alternative to shaping the reflectors is to place a correctly designed lens in front of the feed (Hudson et al. 1987), which has the advantage of being easily removable if desired.

Example of VLA performance In this section I will give some aperture efficiency and radiation pattern data for the VLA as typical examples of the performance of the primary elements of a synthesis array. Table 3-1 shows the predicted values for the various factors discussed above for four of the VLA observing wavelengths.

Table 3-1. VLA Performance Examples

λ	η_{sf}	η_{bl}	η_s	η_t	η_{diff}	η_{misc}	η_{pred}	η_{meas}
20 cm	1.0	.85	.82	.98	.86	.94	.55	.51
6 cm	.97	.85	.92	.98	.96	.94	.67	.65
2 cm	.85	.85	.90	.95	.98	.94	.57	.52
1.3 cm	.68	.85	.90	.95	.99	.94	.46	.43

In Table 3-1 η_{diff}, the diffraction loss of the subreflector, is significant at 20-cm wavelength, where the subreflector is too small; η_{pred} is the total predicted efficiency, the product of the six factors to its left; and η_{meas} is the actual measured efficiency.

A powerful diagnostic measurement for reflector antennas is known as the "holographic" measurement (Scott and Ryle 1977; Mayer et al. 1983; Kraus 1986, section 6-22) and is ideally suited for use on the primary elements of a

synthesis array. This measurement is based on the Fourier transform relationship of Equation 3-7. $F(u,v)$ is measured by scanning one of the antennas, as in Figure 3-1, back and forth across a strong point source while the other antenna continuously tracks the source. $f(x,y)$, the complex aperture distribution of the scanning antenna, is then computed using Equation 3-7. $|f(x,y)|$ then directly shows the aperture blockage and illumination, whilst $\arg(f(x,y))$ provides information about reflector surface errors and feed location errors. Figure 3-11 shows the results of a holographic measurement of a VLA antenna. $|F(u,v)|$ shows the expected sidelobe enhancement in the planes of the subreflector support spars, and $|f(x,y)|$ clearly shows the uniform illumination resulting from the shaped reflectors and the spar blockage.

4.2. Pointing accuracy

The pointing accuracy of an antenna often limits the maximum usable frequency as much as reflector surface accuracy does. The desirable goal for the pointing accuracy, $\Delta\theta$, is $\Delta\theta < \theta_{3dB}/20$ at the highest frequency of operation, where θ_{3dB} is the full width to half maximum power of the antenna beam. With this performance, a source located at the center of the primary beam will suffer negligible intensity variations because $\mathcal{A}(\theta_{3dB}/20) \approx 0.995$. As well as the on-axis intensity variations caused by pointing errors, the effect on a source located well out in the beam is important if extended sources are being imaged. With one-twentieth of a beamwidth pointing errors the fractional intensity variation of a source located at the half power point is $2\mathcal{A}(\theta_{3dB}(\frac{1}{2}+\frac{1}{20})) \approx 0.87$, which will significantly reduce the accuracy of the outer part of the image.

The VLA antenna pointing accuracy is approximately 15 arcseconds. This corresponds to $\sim \theta_{3dB}/7$ at $\lambda = 1.3$ cm, which is quite marginal since it will cause 5% intensity fluctuations at the beam center and 36% variations for a source at the half power point on the beam. One must consider the effect of this pointing error on wide-field images even at low frequencies. For example, at $\lambda = 21$ cm this pointing error causes 2% intensity variations at the half power point, which will be significant for high dynamic range images.

The design of the antenna for good pointing performance requires attention to a large number of details. Structural design for gravitational, wind and thermal loading on the antenna must be done carefully, with the latter two effects being the more important because they are not repeatable and therefore cannot be calibrated. A significant problem is provision of a sufficiently accurate model of the wind and thermal conditions at the array site. As well as deformations of the mount and reflector structure, the positional stability of the feed and subreflector can have a significant impact on pointing (Rudge et al. 1982, p. 169). The accuracy of any bearings and the precision and repeatability of the position transducers on the two axes must be considered. The servosystem and electromechanical drive designs play a major role in pointing accuracy, with wind performance being the most difficult problem. Finally, it is important to have a sufficiently accurate model in the control computer for both repeatable antenna pointing errors and atmospheric refraction. The coefficients of the antenna model are determined by measuring, on a periodic basis, the pointing errors on point sources distributed over the sky, and refraction correction requires data from an accurate and reliable weather station.

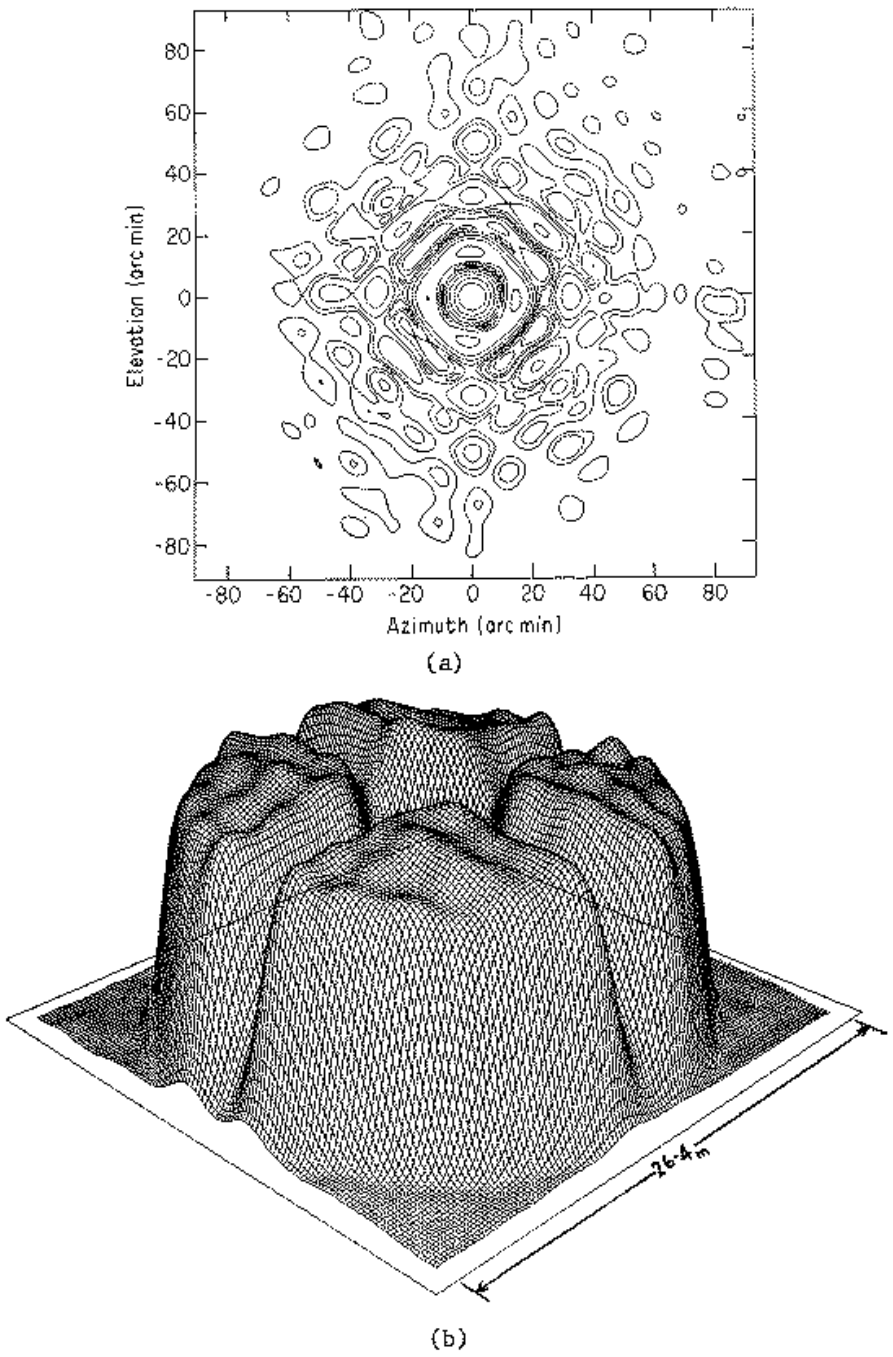

Figure 3-11. Results of a holographic measurement of a VLA antenna at 4.8 GHz. **(a)** $|F(u,v)|$ [from Napier, Thompson and Ekers (© 1983 IEEE)]; **(b)** $|f(x,y)|$. Phases are not shown because, at 4.8 GHz, they show little variation.

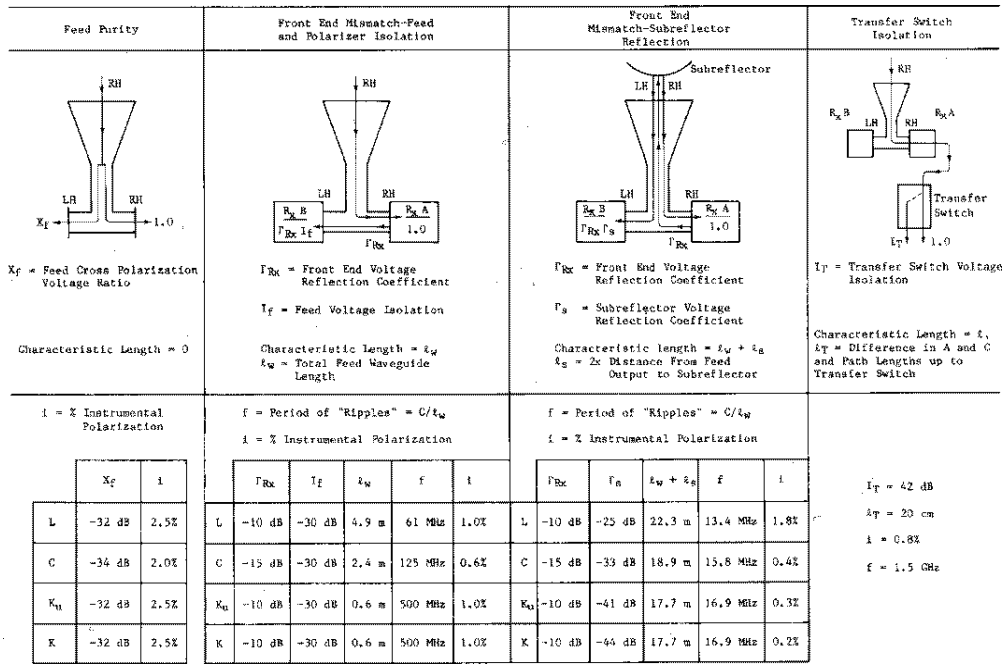

	X_f	i
L	-32 dB	2.5%
C	-34 dB	2.0%
K_u	-32 dB	2.5%
K	-32 dB	2.5%

	Γ_{Rx}	I_f	ℓ_w	f	i
L	-10 dB	-30 dB	4.9 m	61 MHz	1.0%
C	-15 dB	-30 dB	2.4 m	125 MHz	0.6%
K_u	-10 dB	-30 dB	0.6 m	500 MHz	1.0%
K	-10 dB	-30 dB	0.6 m	500 MHz	1.0%

	Γ_{Rx}	Γ_s	$\ell_w + \ell_s$	f	i
L	-10 dB	-25 dB	22.3 m	13.4 MHz	1.8%
C	-15 dB	-33 dB	18.9 m	15.8 MHz	0.4%
K_u	-10 dB	-41 dB	17.7 m	16.9 MHz	0.3%
K	-10 dB	-44 dB	17.7 m	16.9 MHz	0.2%

Figure 3-12. Sources of on-axis instrumental polarization using circularly polarized feeds for the VLA. [From Bignell 1982.]

Pointing performance can be improved if the pointing errors are frequently measured on a calibration source near to the object being imaged. In this observing mode, known as "offset pointing" or "referenced pointing" mode, corrections for the measured pointing errors are continuously applied in the computer pointing model for the antenna. Provided the pointing errors vary sufficiently slowly with time and antenna position, significant improvements in pointing accuracy can be made.

4.3. Antenna polarization properties

At the output of the antenna feed a polarization splitter provides separate output ports for two orthogonal polarizations, either linearly or circularly polarized. A number of mechanisms, discussed below, will prevent the output from a polarization splitter port from providing purely only one polarization component and none of the orthogonal one. The ratio of the undesired orthogonal component to the desired one, expressed as a voltage ratio, is known as the "instrumental polarization", "polarization crosstalk" or "polarization leakage". Instrumental polarization, if its effect is not removed from the data, can have a major effect on the quality of a polarization image. It will make an unpolarized source appear polarized and alter the apparent polarization distribution of a polarized source. The antenna instrumental polarization has two main components, a component at the center of the antenna beam that can be treated as constant across the beam and a component that varies across the beam. I will consider these two components separately.

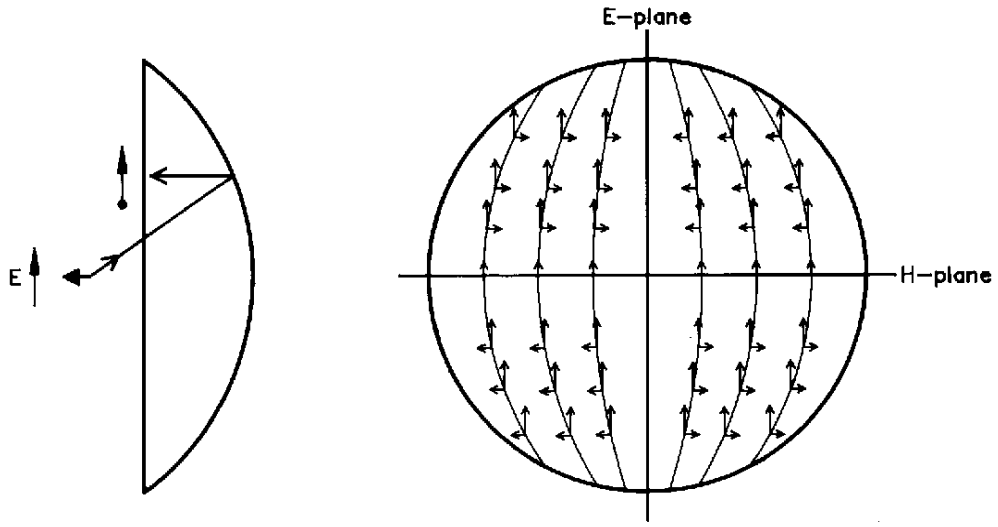

Figure 3-13. Field distribution in the aperture of a paraboloid fed by an electric dipole. The field is resolved into its co- and cross-polarized components.

The cross-polarization component that is constant across the beam is primarily due to the quality of the polarization splitter and, in the case of circular polarization, to reflections in the path between the subreflector and the receiver. The magnitudes of some of these effects for four of the VLA observing bands are shown in Figure 3-12. The goal with these effects is to make them as small as economically feasible and, more importantly, to ensure that they are constant in time so that their effect can be removed using the calibration procedure discussed in Lecture 6.

The cross-polarization component that varies across the antenna beam results from the curvature of the electric field lines in the feed pattern illuminating the main reflector (Rudge et al. 1982, p. 346). The situation is illustrated in Figure 3-13 which shows the electric field in the aperture of a parabola illuminated by an electric dipole. Note that the cross-polarized aperture distribution, $f_c(x, y)$ has the antisymmetric pattern shown schematically in Figure 3-14(a). The average value of $f_c(x, y)$ is zero, so it does not give rise to on-axis instrumental polarization. The cross-polarized radiation pattern, $F_c(u, v)$, which is the Fourier transform of $f_c(x, y)$, is also shown schematically in Figure 3-14(b). Note the four-lobed structure with the lobe peaks located at approximately the half power point of the primary copolarized beam. Typically these cross-polarized lobes are a few percent of the copolarized response at their peaks. An actual measured $F_c(u, v)$ for a VLA antenna is also shown in Figure 3-14. The effects of $F_c(u, v)$ are not removed by the usual polarization calibration techniques, and significant errors could be introduced into a polarized image of a source comparable in size to the antenna beam. The situation is further complicated on an alt–az antenna because $F_c(u, v)$ rotates with respect to the source, as explained in Section 3.2.. As well as the field curvature described above, four-lobed cross-polarized patterns of this type are also caused by non-circularity of the feed pattern and, to a small extent, by the curvature of the primary reflector.

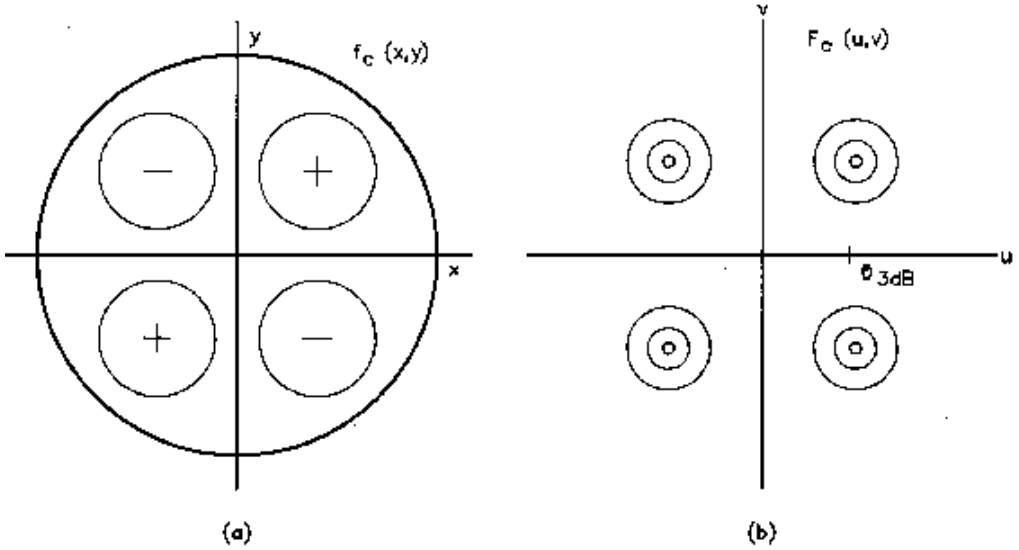

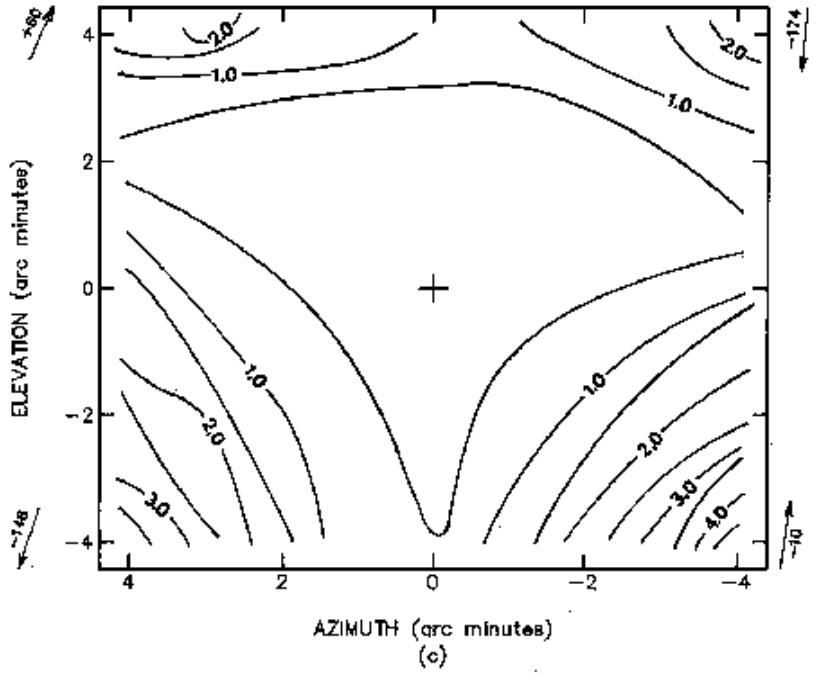

Figure 3-14. Cross-polarized beam of a reflector antenna. **(a)** Schematic diagram of $f_c(x, y)$ corresponding to the cross-polarized field in Figure 3–12. **(b)** Form of $F_c(u, v)$. **(c)** $F_c(u, v)$ measured on a VLA antenna at 4.8 GHz (from Bignell 1982). The half power point of the primary beam is 4.5 arcminutes. The on-axis instrumental term has been subtracted out, and contours are in percent polarization. The lack of symmetry of the four lobes results from the VLA asymmetric antenna geometry.

The peaks of $F_c(u,v)$ can be minimized by using multimode feedhorns, such as corrugated horns (Rudge et al.. 1982, p. 359), which have circularly symmetric patterns and do not have the field curvature problems of a simple electric dipole.

A few words should be said about the effects of loss of symmetry in the antenna geometry. If there is no symmetry in the geometry then the anti-symmetry of Figure 3-14(a) will be lost and the cross polarization will not cancel in the on-axis direction. The off-axis geometry of the VLA, shown in Figure 3-6(c), has a plane of symmetry so the cancellation still occurs on-axis for linear polarization. Cross polarization in this case causes the circularly polarized beams to point in slightly different directions (Chu and Turrin 1973).

References

Balanis, C. A. 1997, *Antenna theory*, Second edition, John Wiley & sons.

Bignell, R. C. 1982, *Polarimetry*, Lecture No. 6 in *Synthesis Mapping: Proceedings of the NRAO–VLA Workshop held in Socorro, New Mexico, June 21–25*, A. R. Thompson and L. R. D'Addario, Eds., NRAO (Green Bank, WV).

Chu, T. S. & Turrin, R. H. 1973, "Depolarization properties of offset reflector antennas", *IEEE Trans. Ant. Propagat.*, **AP-21**, 339–345.

Hansen, R. C., Ed. 1964, *Microwave Scanning Antennas*, Volume 1, Academic Press, New York.

Hudson, J., Plambeck, R., & Welch, W. J. 1987,"Aperture efficiency enhancement in a Cassegrain system by means of a dielectric lens", *Radio Science*, **22**, 1091–1101.

Kraus, J. D. 1986, *Radio Astronomy*, Second Edition, Cygnus-Quasar Books (Powell, Ohio).

Kraus, J. D. 1988, *Antennas, 2nd Ed.*, McGraw-Hill.

Mayer, C. E., Davis, J. H., Peters, W. L., & Vogel, W. J. 1983,"A holographic surface measurement of the Texas 3.9-m antenna at 86 GHz", *IEEE Trans. Instrum. Meas.*, **IM-32**, 102–109.

Napier, P. J., Thompson, A. R., & Ekers, R. D. 1983, "The Very Large Array: Design and performance of a modern synthesis radio telescope", *Proc. IEEE*, **71**, 1295–1320.

Olver, A. D., Carricoats, P. J. B., Kishk, A. A. & Shafai, L. 1994, *Microwave horns and feeds*, IEE Electromagnetic Waves series vol 39.

Rudge, A. W., Milne, K., Olver, A. D., & Knight, P., Eds. 1982, *The Handbook of Antenna Design*, Volume 1, Peter Peregrinus, London.

Ruze, J. 1966, "Antenna tolerance theory—A review", *Proc. IEEE*, **54**, 633–640.

Scott, P. F. and Ryle, M. 1972, "A rapid method for measuring the figure of a radio telescope reflector", *Mon. Not. Roy. Astron. Soc.*, **178**, 539–545.

Thompson, A. R., Moran, J. M., and Swenson, G. W., Jr. 1986, *Interferometry and Synthesis in Radio Astronomy*, John Wiley & Sons, New York.